The Role of Conservation of Mass in the Satellite-Derived Poleward Moisture Transport over the Southern Ocean

CHENG-ZHI ZOU

QSS Group, Inc., Lanham, Maryland, and U.S. National Ice Center, Washington, D.C.

MICHAEL L. VAN WOERT

Office of Research and Applications, NOAA/NESDIS, Camp Springs, Maryland, and U.S. National Ice Center, Washington, D.C.

(Manuscript received 28 December 1999, in final form 12 June 2000)

ABSTRACT

Poleward meridional moisture transport across the Southern Ocean during 1988 is investigated by applying conservation of mass to the wind derivation approach of Slonaker and Van Woert. The moisture field is from the Television and Infrared Observational Satellite (TIROS) Operational Vertical Sounder (TOVS) Pathfinder A dataset. The wind field is first derived from a combination of the TOVS temperature profiles and a satellite-based surface wind field using the thermal wind relationship. Then a Lagrange multiplier is introduced in a variational procedure to constrain the wind to conserve mass.

The introduction of the conservation of mass reduces the estimates of the moisture flux and net precipitation dramatically in comparison with the nonmass-conserved method in Slonaker and Van Woert. For instance, the estimates of the zonally averaged, vertically integrated moisture flux across 50°S are reduced by 56% and the net precipitation between the 50°S and 60°S latitude belt are reduced by 63%. The reason for the difference is that the nonmass-conserved approach leads to unrealistically strong annual-mean winds in the lower troposphere, which results in an exaggerated mean moisture transport. In contrast, the mass-conserved annual-mean wind compares favorably with the radiosonde observations at Macquarie Island and European Centre for Medium-Range Weather Forecasts and National Centers for Environmental Prediction–National Center for Atmospheric Research reanalyses, and it yields a mean moisture flux consistent with historical estimates.

In contrast, the satellite-derived eddy moisture flux is underestimated by about 45% when compared with the radiosonde and analysis studies. This underestimation is probably due to the lower spatial and temporal resolutions of the satellite observations and lack of certain types of ageostrophic winds in the wind derivation.

1. Introduction

Precipitation over Antarctica is recognized as an important climatic variable. It plays a major role in the mass budget of the Antarctic ice sheets balancing mass wastage by iceberg calving and melting. The Antarctic ice sheets are probably in a state of constant imbalance because the timescales for precipitation and ice-sheet wastage are different—precipitation is an atmospheric process and may vary rapidly over time, while the ice-sheet response is controlled by the ocean circulation (Jacobs et al. 1992), which varies over much longer timescales. The imbalance of mass may have a significant impact upon the global sea level change because net fresh water can be either extracted from or released into the global ocean. Whether the imbalance can develop into ice cap instability is a subject of many studies (e.g., Huang and Bowman 1992). Viewed as an isolated process, Antarctic precipitation extracts fresh water from the global ocean. The current best estimate of the annual precipitation rate of Antarctica is about 157 mm yr^{-1} (Bromwich et al. 1995), equivalent to an approximately 7 mm yr^{-1} decrease in sea level. Any changes in the precipitation rate could have important implications with respect to global sea level rise, which is currently estimated to be 1–3 mm yr^{-1} (Douglas 1991).

Precipitation observations over Antarctica are extremely difficult to make due to the lack of radiosonde stations, large errors caused by small rainfall amounts, and drifting snow (Bromwich 1988). Because of the observational difficulties, many studies have concentrated on indirect calculations of the net precipitation using radiosonde observations (raob) or model outputs as inputs into the water vapor budget equation. Peixóto and Oort (1983) used a 10-yr period (1963–73) of raob

Corresponding author address: Dr. Michael Van Woert, NOAA/NESDIS/ORA, NOAA Science Center, 5200 Auth Road, Room 711, Camp Springs, MD 20746.
E-mail: mvanwoert@nesdis.noaa.gov

data to determine the zonal and meridional moisture transport. Bromwich et al. (1995) and Cullather et al. (1996, 1998) performed comprehensive studies of the net precipitation and its long-term change in Antarctica using model analyses. Broad disagreement between the various analyses was observed. For instance, Bromwich et al. (1995) show that the Antarctic annual-mean net precipitation calculated by the European Center for Medium-Range Weather Forecasts (ECMWF), the National Meteorological Center (NMC), and the Australian Bureau of Meteorology (ABM) model analyses ranged from 93 to 190 mm yr^{-1} for 1992. Some of the net precipitation change in Antarctica has been related to the El Niño–Southern Oscillation (ENSO) phenomenon (Cullather et al. 1996). However, the interannual variability of the net precipitation is also strongly model/analysis dependent. Cullather et al. (1996) show close relationship between ENSO and the ECMWF operational product analyses, while Genthon and Krinner (1998) found no convincing correlation between ENSO and the ECMWF reanalysis data. It is a matter of ongoing debate as to the relative merits of using analysis and reanalysis products in Antarctic precipitation studies (Bromwich et al. 2000).

An alternate method is to use satellite observations to study the Antarctic precipitation. Television and Infrared Observational Satellite (TIROS) Operational Vertical Sounder (TOVS) satellite data provide a continuous record of the temperature and specific humidity profiles with nearly total coverage over the Southern Ocean. The moisture flux calculation requires wind profiles, which are not directly measured by the instrument. However, wind profiles can be inferred from the TOVS data under the assumption that the winds are in geostrophic balance by integrating the hydrostatic equation using the observed temperature profiles. Peterson and Horn (1977) and Moyer et al. (1978) derived geostrophic wind estimates from *Nimbus-6* temperature profiles. Carle and Scoggins (1981) provided a detailed comparison of the satellite-derived wind field from Nimbus-6 soundings with radiosonde observations. They found that the satellite-derived geostrophic wind agrees, on the average, with the radiosonde observations to within 5 m s^{-1} for the limited time periods examined. In this method, however, the surface wind is usually derived from an ancillary boundary layer model (Carle and Scoggins 1981). In addition, this method requires an estimate of the surface pressure field. Unfortunately, satellites are not capable of measuring surface pressure with sufficient accuracy to be useful in such studies. Therefore, over the ocean where no in situ surface pressure observations exist, Francis (1994) resorted to the use of numerical weather analyses for an estimate of the surface pressure field.

Another method for deriving the geostrophic wind is to use a tie-on wind (observed known wind) at a specific level in association with the thermal wind equation (Arnold et al. 1976). Recently released, satellite-based surface wind data, produced by Atlas et al. (1993) using a variational analysis method (VAM), provide the first opportunity to use this method to produce a satellite-derived moisture budget for high southern latitudes. Slonaker and Van Woert (1999, hereinafter referred to as SVW99) used this VAM surface wind data along with TOVS temperature soundings to derive meridional wind fields via the thermal wind relationship. Then, the moisture flux and net precipitation over the Southern Ocean were estimated from the derived wind profiles and TOVS moisture data.

Though the SVW99 results are quite encouraging, the thermal wind relationship alone cannot be used to estimate the vertical wind profiles from the observed surface wind field and temperature soundings because it does not conserve mass. The reason for the failure of the system to conserve mass is the ageostrophic component of the surface wind field. That is, the SVW99 method is not a balanced approximation model for the wind derivation. A balanced model of the atmosphere requires at least an approximate form of the horizontal momentum equations along with the hydrostatic equation, continuity equation, and thermal equation (Gent and McWilliams 1983; Boville 1987). In SVW99, the hydrostatic and thermal wind equations are assumed to hold true and the thermal equation is implicitly known; because, the temperature profiles are measured directly by the satellite. However, the continuity equation, which ensures conservation of mass, was not considered by SVW99. Conservation of mass represents a strong constraint on the wind field, especially for the long-term averaged climate states such as the annual-mean circulation.

In this study a variational technique is developed to derive the mass-conserved wind field. In the variational procedure, the meridional wind is obtained by the thermal wind assumption in conjunction with the satellite-observed atmospheric temperature profiles and surface wind. Meanwhile, a Lagrange multiplier is introduced to constrain the wind to conserve mass. A detailed comparison of the derived wind profiles against radiosonde observations and reanalyses is also carried out. It will be shown that after the introduction of conservation of mass, the calculated moisture flux and net precipitation are dramatically reduced and improved with respect to the SVW99 estimates.

The next section describes the data used in this study. In section 3, we describe the variational method used to obtain a mass-conserved wind field. Section 4 compares the computed wind field with reanalysis and raob data. In section 5 the detailed characteristics of the satellite-derived moisture fluxes are described. Section 6 calculates the net precipitation from the moisture flux, and section 7 provides a summary and discussion.

2. Data

The data used in this study are the same 1988 data used by SVW99. The surface wind velocities are taken from Atlas et al. (1993) who ''fused'' Special Sensor

Microwave Imager (SSM/I) surface wind speed, in situ observations, and ECMWF analyses using a variational method. These surface wind vectors, referred to as VAM winds, exhibit higher accuracy than values from the ECMWF analysis alone when compared with independent buoy data (Atlas et al. 1996).

The moisture and temperature data are from the TOVS Pathfinder Path A dataset (Susskind et al. 1997). There are two moisture datasets in the TOVS Pathfinder A: one is the specific humidity obtained by a physical retrieval method at mandatory levels and the other is the layer precipitable water integrated from the specific humidity profile. In SVW99, as well as in this study, the layer precipitable water dataset is used. This dataset has five layers: surface–850, 850–700, 700–500, 500–300, and 300–100 hPa. Because the lowest precipitable water layer is from the surface to 850 hPa, the moisture flux obtained in this study includes the effect of the thin moist surface layer. The layer mean virtual temperature is defined at the same layers as the layer precipitable water except that the lowest layer is taken from 1000 to 850 hPa. These moisture and temperature data are provided on a $1^\circ \times 1^\circ$ latitude and longitude grid and have been interpolated by SVW99 onto a 2° latitude by 2.5° longitude grid with a 6-h interval to match the surface wind data of Atlas et al. (1993).

3. Derivation of the mass-conserved satellite wind

The continuity equation in an atmosphere of hydrostatic balance and in spherical and isobaric coordinates is written as (e.g., Peixóto and Oort 1992)

$$\frac{\partial u}{a\cos\varphi\partial\gamma} + \frac{\partial(v\cos\varphi)}{a\cos\varphi\partial\varphi} + \frac{\partial\omega}{\partial p} = 0, \tag{1}$$

where a is the earth's radius, γ is the longitude, φ is the latitude, and p is the pressure; u, v, and ω are zonal, meridional, and vertical p velocities, respectively. In both SVW99 and this study, only the meridional velocity is derived. Integrating Eq. (1) over a latitude circle, over p from the surface $p = p_0$ to the top of the atmosphere $p = 0$, and over latitude from a pole to latitude φ, assuming boundary conditions $\omega = 0$ at $p = 0$ and $p = p_0$, and $v = 0$ at the poles, one obtains the conservation equation of mass for the meridional velocity,

$$\int_0^{p_0}\int_0^{2\pi} va\cos\varphi\, d\gamma\, dp = 0. \tag{2}$$

This integration constraint has to be satisfied by any derivation method of the meridional wind for long-term climate studies. For a pure geostrophic approximation, Eq. (2) is satisfied because the meridional geostrophic wind is related to the longitudinal derivative of the geopotential height that vanishes when integrated over a latitude circle. In SVW99 as well as this study, the thermal wind approximation is used to derive the meridional wind from the satellite temperature soundings and surface wind field. The thermal wind relationship for the meridional wind is

$$\frac{\partial v_g}{\partial \ln p} = -\frac{R_d}{f}\frac{\partial T_v}{a\cos\varphi\partial\gamma}, \tag{3}$$

where f is the Coriolis parameter, R_d is the dry air gas constant, v_g is the geostrophic meridional wind speed, and T_v is the virtual temperature. At a particular level p, SVW99 used the following formula, derived by vertically integrating Eq. (3), to estimate the meridional wind,

$$\tilde{v} = v_0 + \int_p^{p_0}\frac{R_d}{f}\frac{\partial T_v}{a\cos\varphi\partial\gamma}\, d\ln p, \tag{4}$$

where $\tilde{v}$ is the SVW99 wind and v_0 is the VAM surface wind (Atlas et al. 1993). Because the integration of $\partial T_v/(a\cos\varphi\partial\gamma)$ over a latitudinal circle vanishes, the integration of Eq. (4) over altitude and longitude reduces to

$$\int_0^{p_0}\int_0^{2\pi}\tilde{v}a\cos\varphi\, d\gamma\, dp = p_0\int_0^{2\pi} v_0 a\cos\varphi\, d\gamma. \tag{5}$$

Equation (5) indicates that, because the longitudinal integration of v_0 is not zero, mass is not conserved for the wind $\tilde{v}$.

In this study a Lagrange multiplier is introduced to constrain the total mass in a latitudinal circle. This process is similar to that of Gruber and O'Brien (1968), who used a Lagrange multiplier to constrain the total mass divergence in a least squares polynomial smoothing process on the radiosonde winds. Given $N + 1$ levels in the vertical direction and $M + 1$ grid points in a zonal circle and using the trapezoidal rule, the grid point forms of Eqs. (4) and (2) at any latitude φ are written as

$$\tilde{v}_{i,k} = v_{i,0} + \sum_{n=1}^{k}\frac{R_d}{f}\frac{\partial T_{vi,n-1/2}}{a\cos\varphi\partial\gamma}\ln\left(\frac{p_{n-1}}{p_n}\right), \qquad i = 0, 1, \ldots, M, \qquad k = 1, 2, \ldots, N \tag{6}$$

and

$$\sum_{i=0}^{M}\sum_{k=0}^{N-1}\frac{1}{2}(v_{i,k} + v_{i,k+1})a\cos\varphi\Delta\gamma\Delta p_k = 0, \tag{7}$$

where i is the index of the zonal grid point, k and n are the indexes of the vertical level, $\Delta p_k = p_k - p_{k+1}$ (the difference of pressures between the two levels k and $k + 1$), $v_{i,k}$ is the mass-conserved meridional wind speed at the grid point (i, k), and $\Delta\gamma$ is the longitudinal grid interval. Using the layer mean virtual temperature profiles from TOVS and the VAM surface wind, and assuming the surface pressure to be 1000 hPa, the upper-level nonmass-conserved wind, $\tilde{v}$, can be first determined from Eq. (6) at 850-, 700-, 500-, 300-, and 100-hPa levels. Then the mass-conserved wind, v, can be obtained by a variational formalism in which the differences between v and $\tilde{v}$ are minimized in a least

squares sense subject to the mass conservation constraint. The variational formalism using Eq. (7) as a strong constraint is written as follows [e.g., Daley (1991) and its references for the general construction of variational functionals],

$$E = \sum_{i=0}^{M}\sum_{k=1}^{N}(v_{i,k} - \tilde{v}_{i,k})^2 a\cos\varphi\Delta\gamma + \lambda\sum_{i=0}^{M}\sum_{k=0}^{N-1}\frac{1}{2}(v_{i,k} + v_{i,k+1})a\cos\varphi\Delta\gamma\Delta p_k, \quad (8)$$

where λ is an as yet undetermined Lagrange multiplier. The Lagrange multiplier must be a function of latitude and time. In the vertical and longitudinal directions, however, λ can either be uniform or have a functional form *prescribed* based on physical or observational considerations. For simplicity we assume that λ is uniform on a latitude wall. Comparisons with raob and reanalysis data, which are presented later, suggest this is a valid assumption.

After rearranging the vertical index, Eq. (8) becomes

$$E = \sum_{i=0}^{M} a\cos\varphi\Delta\gamma\left[\sum_{k=1}^{N}(v_{i,k} - \tilde{v}_{i,k})^2 + 2\lambda\sum_{k=0}^{N} f_k v_{i,k}\right], \quad (9)$$

where

$$f_k = \begin{cases} 0.25\Delta p_0, & k = 0 \\ 0.25(\Delta p_k + \Delta p_{k-1}), & k = 1, 2, N-1 \\ 0.25\Delta p_{N-1}, & k = N. \end{cases} \quad (10)$$

The Euler–Lagrange equations derived from Eq. (9) are

$$\frac{\partial E}{\partial v_{i,k}} = a\cos\varphi\Delta\gamma[2(v_{i,k} - \tilde{v}_{i,k}) + 2\lambda f_k] = 0, \quad i = 0, 1, \ldots, M, \quad k = 1, 2, \ldots, N. \quad (11)$$

From Eq. (11), the following solution for the mass-conserved meridional wind is obtained,

$$v_{i,k} = \tilde{v}_{i,k} - f_k\lambda, \quad i = 0, 1, \ldots, M, \quad k = 1, \ldots, N. \quad (12)$$

Equation (12) shows that the mass conservation correction to the nonmass-conserved wind is proportional to the Lagrange multiplier and the coefficients f_k, which depend on the differencing schemes of the mass conservation equation. The f_k values are not necessarily uniform in the vertical direction. For the grid formation in this study, f_k = 75, 87.5, 100, 100, and 50 hPa at 850, 700, 500, 300, and 100 hPa, respectively.

Introducing Eq. (12) into Eq. (7) and noticing $v_{i,0} = \tilde{v}_{i,0}$, λ can be obtained as

$$\lambda = \frac{\sum_{i=0}^{M}\sum_{k=0}^{N} f_k\tilde{v}_{i,k}}{\sum_{i=0}^{M}\sum_{k=1}^{N} f_k f_k}. \quad (13)$$

Equations (6), (10), (12), and (13) provide a complete solution for the mass-conserved meridional wind given the observed virtual temperature profiles and surface wind. In the following section we discuss and compare the results with radiosonde observations and the ECMWF and the National Centers for Environmental Prediction–National Center for Atmospheric Research (NCEP–NCAR) reanalyses.

4. Comparisons with raob and reanalysis data

a. Comparisons with reanalysis data

Figures 1a–d show, respectively, the nonmass-conserved and mass-conserved satellite winds, the ECMWF reanalysis winds (ERA-15) (Gibson et al. 1996), and the NCEP–NCAR reanalyses (Kalnay et al. 1996). The model based ECMWF and NCEP–NCAR reanalyses approximately conserve mass. They show a low-level convergence and upper-level divergence near 63°S, corresponding to the intersection of the Ferrel and polar cells. In addition, the zonally averaged meridional wind at the top of the boundary layer is weak. The mass-conserved satellite wind reproduces the basic features of the atmospheric circulation, that is, a low-level convergence and upper-level divergence (except at the top level) near 63°S. In contrast, however, the nonmass-conserved satellite wind shows convergence at all levels near 63°S and very strong wind speeds above the boundary layer, which are obviously incorrect. Note that theoretically, the zonally averaged $\tilde{v}$ should be equal to zonally averaged v_0 because the integration of $\partial T_v/(a\cos\varphi\partial\gamma)$ over a latitudinal circle vanishes. However, due to some missing data in the observations, the zonally averaged $\tilde{v}$ is not exactly equal to zonally averaged v_0.

Between 50°S and 63°S, the amplitude of the satellite surface wind is intermediate to the ECMWF and NCEP–NCAR products and the thickness of the poleward-moving boundary layer is very close to the NCEP–NCAR data. Poleward of 63°S, the amplitude of the satellite surface wind is close to the ECMWF data, but the boundary layer thickness in the equatorward moving wind regime is about 100 hPa less than both ECMWF and NCEP–NCAR data. This is most likely because the satellite wind is an average over the ocean area while the ECMWF and NCEP–NCAR data are averages over the whole latitude circle, which contains both ocean and land. The continental elevation is approximately 2 km above sea level, which could lift the boundary layer and thus increase the boundary layer thickness. Considering this factor, it appears that the boundary layer thickness of the mass-conserved satellite wind compares favorably with the reanalyses, especially over the oceans.

Near 63°S, the satellite-derived wind and ECMWF and NCEP–NCAR data all show a boundary layer convergence. This is consistent with the annually and zonally averaged sea level pressure (SLP) as shown in Fig. 2. It is seen in Fig. 2 that there is a low-pressure center

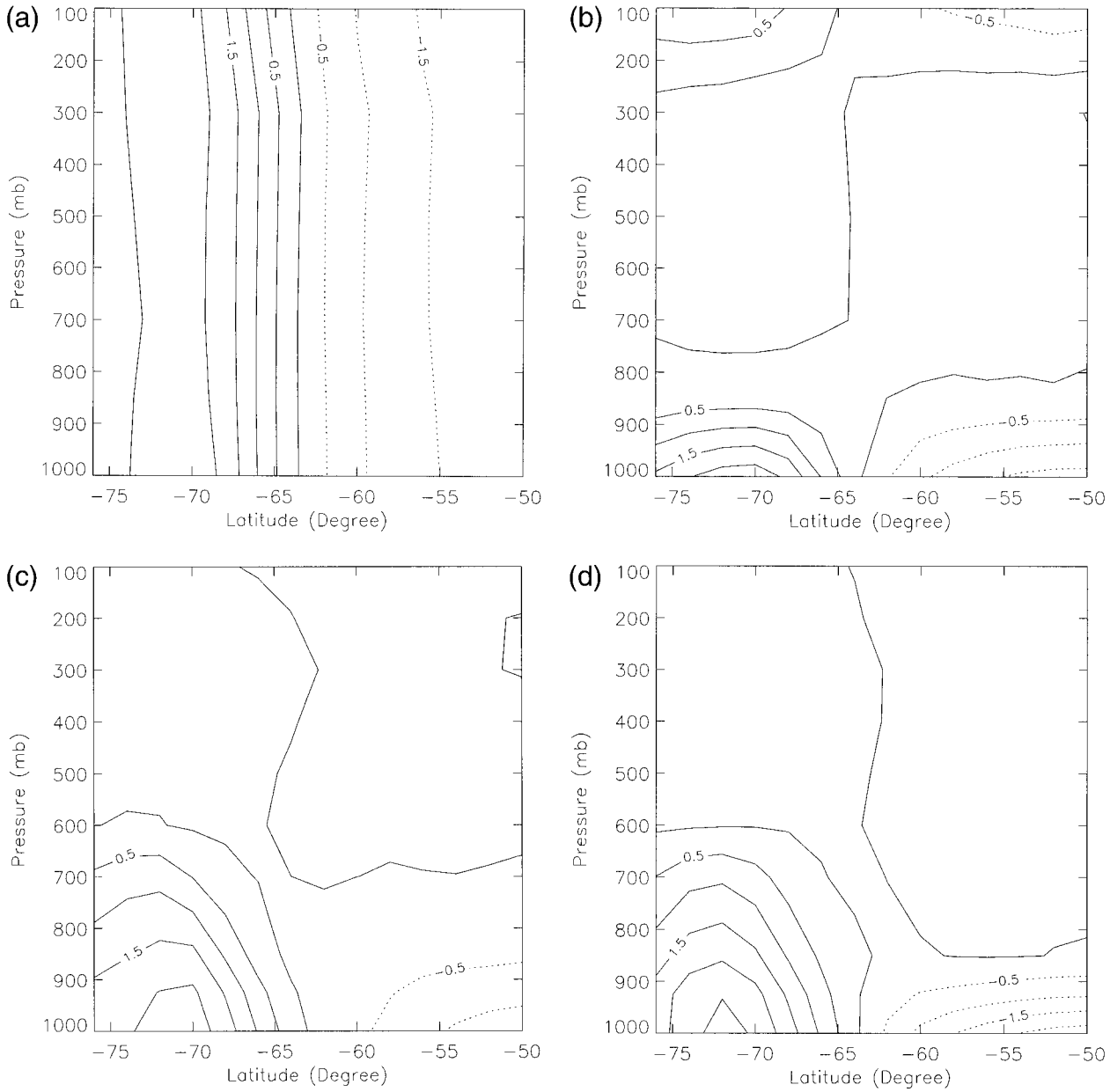

FIG. 1. 1988 annually and zonally averaged meridional winds for (a) satellite-derived, nonmass-conserved; (b) satellite-derived, mass-conserved; (c) ECMWF reanalysis; (d) NCEP–NCAR reanalysis. Contour interval is 0.5 m s^{-1}.

near 63°S where the convergence center is located. This suggests that the convergence in the planetary boundary layer is driven primarily by the pressure gradient.

b. Comparisons with raob data at Macquarie Island

Radiosonde data can be used to assess the overall quality of the satellite-derived data products. In particular, twice-daily wind and moisture soundings are available for 1988 at Macquarie Island (54.5°S, 158.9°E). SVW99 compared the satellite-derived time series of the vertically integrated moisture flux with the radiosonde observations at Macquarie Island. However, they did not provide detailed separate comparisons for the wind and moisture. In the following, a detailed comparison for the wind and moisture profiles between the radiosonde observations and satellite-derived products at Macquarie Island is provided.

1) MERIDIONAL WIND

Table 1 lists the detailed statistics of the comparisons between the raob and satellite-derived winds by both nonmass-conserved and mass-conserved approaches.

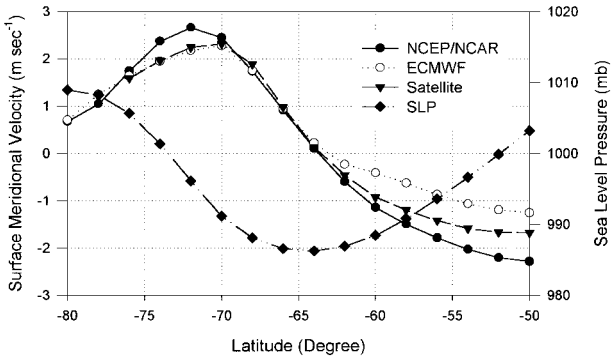

FIG. 2. Comparisons between the yearly and zonally averaged sea level pressure and the yearly and zonally averaged surface meridional winds for 1988.

Figures 3a–c show the scatterplots between the raob and mass-conserved satellite wind for 1000, 850, and 700 hPa, respectively. The scatterplots of the nonmass-conserved winds against raob (not shown here) are similar to Fig. 3 except the mean values are different. The satellite winds at Macquarie Island are obtained by interpolating the values at the four surrounding grid points. Figure 3 and Table 1 show that the wind fields compare most favorably at the surface. Near the surface, the correlation between the satellite wind and radiosonde observations is 0.87 and the rms (root mean square) error is 2.9 m s^{-1}, comparable with the accuracy estimation of ± 2 m s^{-1} for the VAM surface wind (Atlas et al. 1993). For the available data, both raob and satellite yield an annual-mean wind speed of -2.26 m s^{-1} near the surface. This excellent agreement between the raob and satellite winds is probably because Atlas et al. (1993) have incorporated the raob data into the VAM surface wind field.

The correlation between the raob and satellite-derived winds decreases and the rms error increases with increasing height. The rms error increases from 2.9 m s^{-1} at the surface to about 12 m s^{-1} at 300 hPa, which is consistent with the analyses of Carle and Scoggins (1981) in a comparison between the satellite-derived wind using *Nimbus-6* satellite soundings and radiosonde observations. Table 1 also shows that the standard deviation of the nonmass-conserved wind is close to the mass-conserved satellite wind. The standard deviation of both the raob and satellite-derived winds increases with increasing height, except for the 100-hPa level. These increases reflect the increase in the wind speed toward the upper troposphere. The increase in the rms error is partly related to the increase in the standard deviation of both the raob and satellite-derived winds.

It is important to note that, except at the 1000-hPa and 100-hPa levels, the standard deviation of the satellite-derived winds is about 3 m s^{-1}, or 20%–35%, depending on the level, smaller than the raob values. This indicates that the satellite-derived eddy wind speeds underestimate the true wind speeds. There are two possible reasons for the underestimation of the eddy wind field. One is that the raob winds are point data while the satellite winds are spatially and temporally averaged. Because TOVS Pathfinder A data have a resolution of $1° \times 1°$ in both latitude and longitude directions, the spatial average is roughly taken over an area of 64 km (latitude) $\times$ 111 km (longitude) at 54.5°S. Moreover, the data are temporally averaged over a 24-h period (Susskind et al. 1997). This averaging process most likely reduces the variability of the actual wind field. The second reason for the underestimation could be the lack of certain types of ageostrophic wind components in the derivation of the upper-level winds from the TOVS data. As mentioned earlier, only the surface wind contains an ageostrophic wind component in the wind derivation. This surface ageostrophic wind emerges in the upper atmosphere by linearly adding to the thermal wind and readjustment through the conservation of mass. However, this ageostrophic wind may not represent all ageostrophic processes in the atmosphere. For instance, the upper-level ageostrophic winds induced by geostrophic-momentum approximation (e.g., Bluestein 1993) or the ageostrophic acceleration itself could be

TABLE 1. Meridional wind statistics for the raob and satellite-derived data at Macquarie Island for 1988, where ''this study'' refers to the mass-conserved product and SVW99 to the nonmass-conserved product.

	Height					
	1000 mb	850 mb	700 mb	500 mb	300 mb	100 mb
Points	523	539	538	532	510	409
Raob mean (m s^{-1})	−2.26	−1.28	−1.24	−1.08	−2.42	−1.02
Satellite mean (this study) (m s^{-1})	−2.26	−0.94	−0.93	−1.04	−1.93	−1.44
Satellite mean (SVW99) (m s^{-1})	−2.26	−2.41	−2.64	−3.00	−3.90	−2.44
Raob std dev (m s^{-1})	5.69	9.37	10.88	14.25	18.70	9.15
Satellite std dev (this study) (m s^{-1})	5.66	6.13	7.98	11.60	14.45	9.54
Satellite std dev (SVW99) (m s^{-1})	5.66	6.30	8.18	11.86	14.68	9.62
Correlation (raob, this study)	0.87	0.82	0.79	0.77	0.77	0.54
Correlation (raob, SVW99)	0.87	0.82	0.79	0.77	0.77	0.55
Rms (raob, this study) (m s^{-1})	2.89	5.54	6.73	9.09	11.90	8.95
Rms (raob, SVW99) (m s^{-1})	2.89	5.63	6.88	9.29	11.29	9.05
Bias(raob − sat) (this study) (m s^{-1})	0.0	−0.34	−0.30	−0.04	−0.49	0.43
Bias (raob − sat) (SVW99) (m s^{-1})	0.0	1.13	1.41	1.92	1.48	1.42

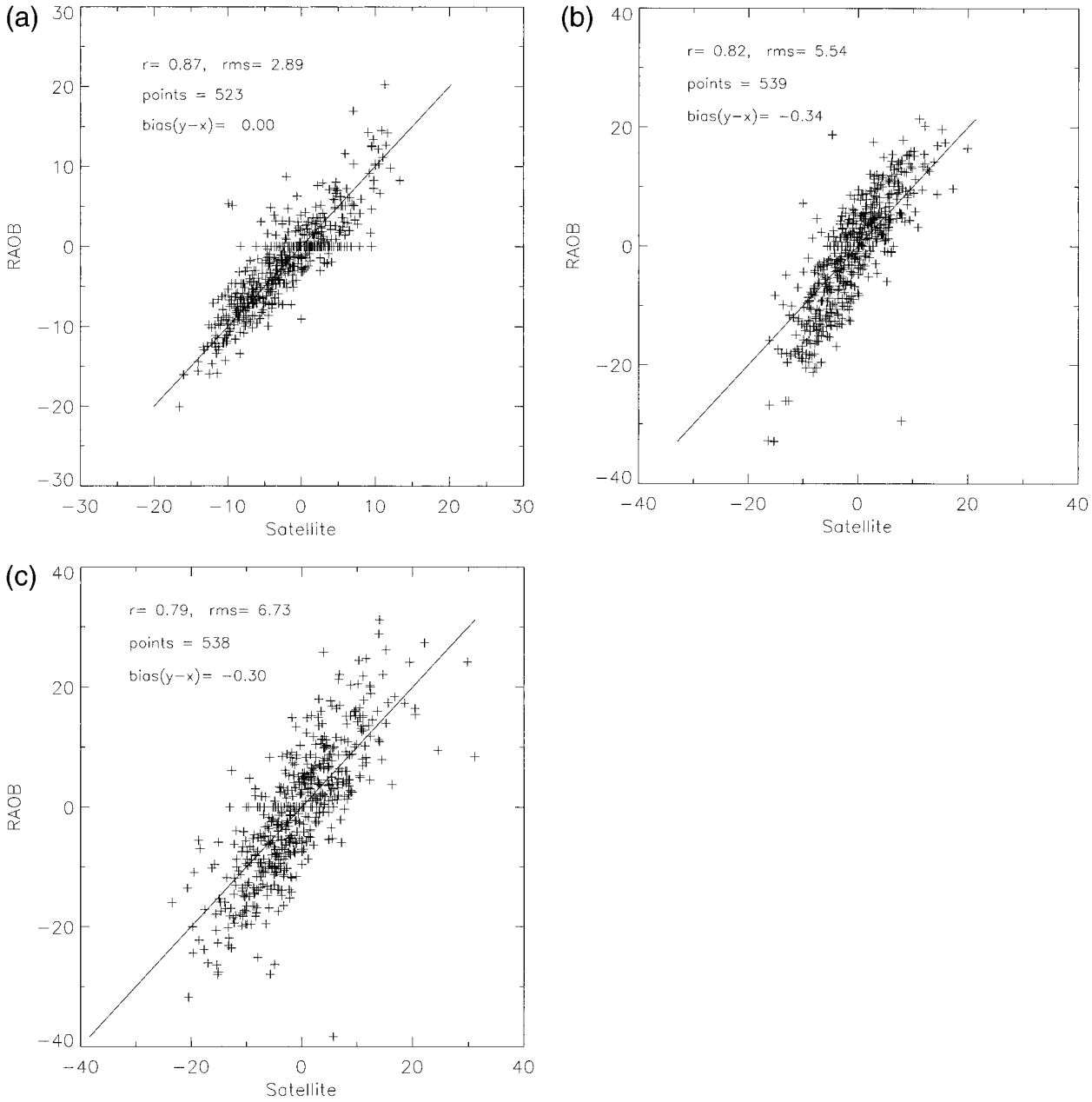

FIG. 3. Scatterplots of the satellite-derived, mass-conserved meridional wind vs radiosonde observations for 1988 at Macquarie Island: (a) 1000, (b) 850, and (c) 700 hPa. Wind speed unit: m s^{-1}.

very important in certain situations. Shapiro and Kennedy (1981) observed in aircraft measurements that the ageostrophic wind could be extremely strong near fronts and the jet stream because the parcel trajectories were sharply curved, indicating significant geostrophic and ageostrophic accelerations. In these situations, other approximations such as quasigeostrophic or semi-quasigeostrophic models might be more appropriate.

Compared with the study of SVW99, the most significant improvement for the mass-conserved satellite winds over the nonmass-conserved winds is in the annual-mean wind field. The mass-conserved annual-mean satellite winds agree with the raob winds to within 27%, while the annual-mean winds of SVW99 are typically 100% stronger than the raob mean winds. As will be shown later, this improvement will have a significant influence on the mean moisture fluxes. It is also noted that the mass-conserved, annually and zonally averaged satellite winds disagree with the ECMWF and NCEP–NCAR reanalyses at 100 hPa (Fig. 1). In particular, both the ECMWF and NCEP–NCAR reanalyses show a weak northward annually and zonally averaged wind at 100

hPa between 50°S and 63°S, indicating that the upper branch of the Ferrel cell extends to the tropopause. In contrast, the satellite-derived wind is strongly southward in this region, showing a second reversed cell above the Ferrel cell. Some observations do indicate a reversed cell appearing above the Ferrel cell (e.g., Oort and Peixóto 1983). However, because of the lack of radiosonde observations in this region, the zonal mean results must be viewed with caution. Although the satellite-derived winds disagree with the reanalyses at 100 hPa, they do agree fairly well with the raob data at 100 hPa as shown in Table 1. As mentioned earlier, we have assumed a constant Lagrange multiplier in the wind derivation. This result indicates that the assumption of a uniform Lagrange multiplier in the vertical and longitudinal directions is appropriate compared to the raob observations at Macquarie Island. However, a constant λ is inappropriate near the tropopause based on comparisons with the reanalyses. To resolve this discrepancy, more raob observations as well as diagnostic studies of the reanalyses are required in this region. Regardless, this discrepancy has little impact on the moisture flux because there is little moisture in the upper troposphere; however, it may have important implications with respect to the heat budget because a significant portion of the sensible heat is transported near the tropopause (Oort ahd Peixóto 1983).

2) MOISTURE

The moisture comparison is made for the specific humidity at the surface, 850-, 700-, 500-, and 300-hPa levels. The satellite-derived specific humidity is obtained from the layer precipitable water based on the integral relationship between the two quantities (e.g., Bromwich et al. 1995). The trapezoidal rule is used for the integration. The integration requires that the specific humidity at 100 hPa and the surface pressure be known. At Macquarie Island, the radiosonde-measured annual-mean surface pressure for 1988 is 997 hPa with a standard deviation of 5 hPa. We therefore assume that the surface pressure, p_0, is 1000 hPa and that the specific humidity at 100 hPa is zero. Figures 4a–c show scatterplots of the specific humidity between the 1988 raob data from Macquarie Island and the satellite retrievals for the surface, 850-, and 700-hPa levels, respectively. Table 2 lists the statistics of this comparison. This 12-h data comparison indicates large discrepancies between the satellite retrievals and radiosonde observations. The following discusses some general characteristics of this comparison.

The annual means of the satellite retrievals from *NOAA-10* are about 10% larger than the raob values below 700 hPa, but about 30% smaller than the raob above 500 hPa. Susskind et al. (1997) indicate that *NOAA-10* produces larger moisture values in the lower troposphere compared to SSM/I and *NOAA-11* retrievals, so the larger satellite-retrieved moisture values presented here are consistent with Susskind et al.'s results. The larger differences observed in the upper troposphere are to be expected because the moisture is typically small and difficult to measure there.

In addition, with the exception of the surface layer, the variability portrayed by the satellite data is generally less than the raob data by 20%–30%. The reason could be, as discussed earlier in the wind comparison, the raob data are point data while the satellite data are spatially and temporally averaged. At the surface, however, the variability of the satellite data is larger than the raob data. This may be related to the local structure of the raob data. For example, at the surface, horizontal transfer is constrained by surface friction so the raob data represent the characteristics of the local land, which is probably drier than the surrounding oceans that the satellite retrievals represent.

The correlation between the raob data and satellite retrievals is above 0.5 for every level except at 850 hPa. The rms error is largest (1.5 g kg^{-1}) at 850 hPa, which is consistent with the findings of Wang et al. (1995). They attribute this to the rapid day-to-day variations of the boundary layer.

Above 850 hPa, there is an obvious asymmetry in the satellite retrievals. The satellite retrievals tend to be larger than the raob observations when the moisture is low and smaller than the raob when the moisture is higher. At present, it is difficult to discern the reasons for this discrepancy; however, it has been shown that the humidity retrievals depend strongly on the first-guess profiles, especially near the surface (Reuter et al. 1988). If this is the case, then refinements to the TOVS products such as the planned Pathfinder Path-B (Susskind et al. 1997) may correct this deficiency.

3) MOISTURE FLUX

The total moisture flux is divided into eddy and mean moisture fluxes. The detailed statistical analyses of the wind and moisture fields described in the previous subsections provide a better understanding of the moisture transport process. Figures 5a–c show the scatterplots between the raob and satellite-derived moisture fluxes at the surface, 850-hPa and 700-hPa levels, respectively. Figure 5d is the vertically integrated total moisture flux. Table 3 summarizes the statistical comparisons of the raob data and satellite-derived moisture fluxes. This comparison reveals some advantages as well as some disadvantages of using satellite data for moisture flux studies. The following discussion concentrates only on the lower atmosphere because the upper troposphere contributes little to the vertically integrated moisture transport.

In comparing Table 3 with Tables 1 and 2, it is seen that the correlation between the raob and satellite-derived moisture fluxes is smaller than the wind correlation, but much better than the moisture correlation. This suggests that the wind correlation dominates the flux

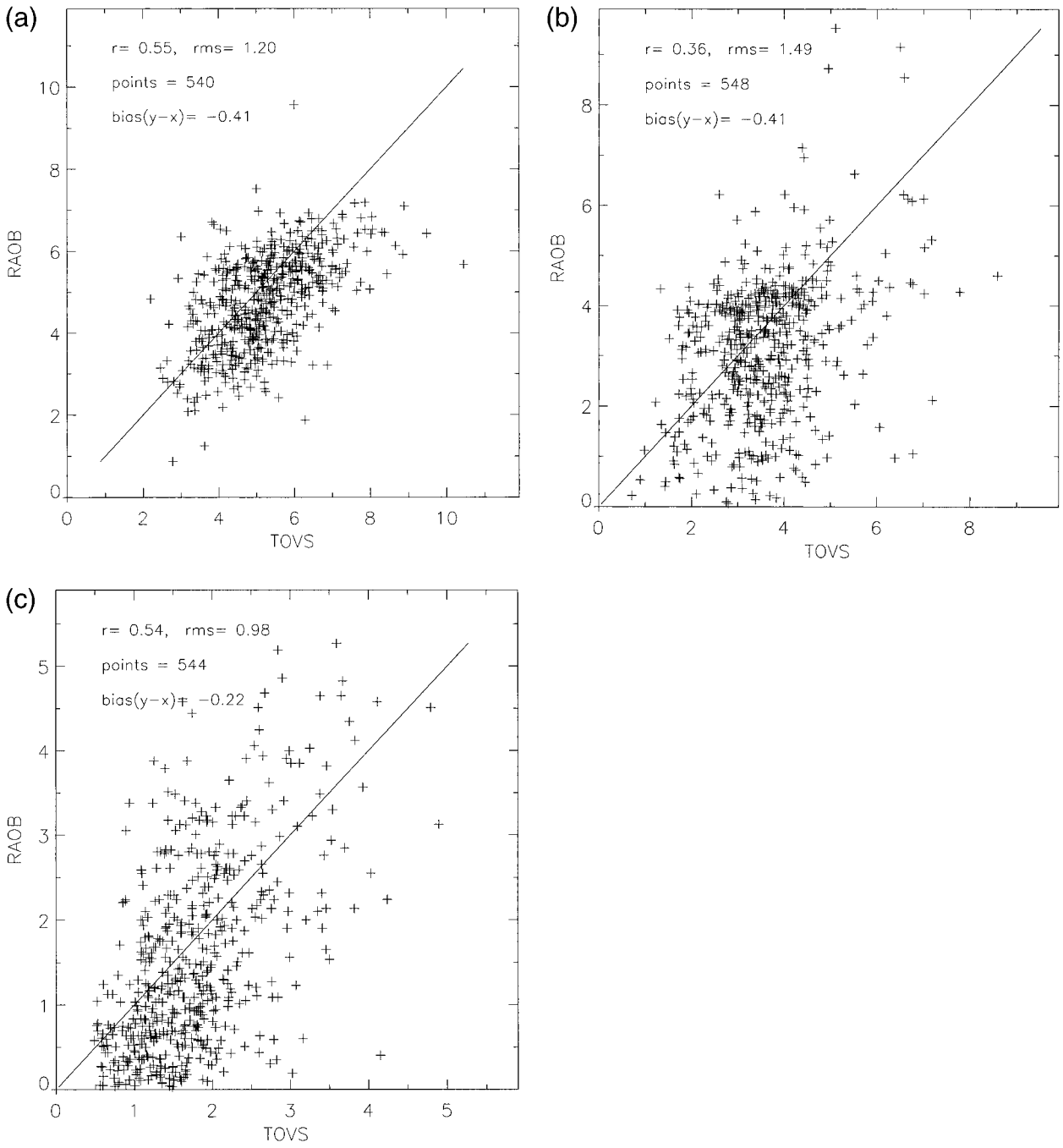

FIG. 4. Scatterplots of the satellite-retrieved specific humidity vs radiosonde observations for 1988 at Macquarie Island: (a) 1000, (b) 850, and (c) 700 hPa. Unit: g kg^{-1}.

correlation. Therefore, although the moisture retrievals have larger disagreement with the raob data as discussed in the previous subsection, a reasonable moisture flux can still be obtained provided accurate wind profiles are available.

The agreement between the raob and satellite-derived mean fluxes with a mass-conserved wind in the lower atmosphere is typically within 10%–20%. The vertically integrated mean flux for this study is -17.8 kg m^{-1} s^{-1}, which is in excellent agreement (within 6%) with the raob value of -19.0 kg m^{-1} s^{-1}. This is probably due to the good agreement of both the annual-mean wind and moisture fields in the lower atmosphere. The mean fluxes of SVW99 are over 100% larger than the raob values at 850, 700, and 500 hPa, which results in a large vertically integrated mean moisture transport. Those

TABLE 2. Specific humidity statistics between the raob data and satellite retrievals at Macquarie Island for 1988.

	Height				
	1000 mb	850 mb	700 mb	500 mb	300 mb
Points	540	548	544	536	518
Raob mean (g kg^{-1})	4.77	3.16	1.52	0.48	0.04
Satellite mean (g kg^{-1})	5.17	3.56	1.75	0.32	0.03
Raob std dev (g kg^{-1})	1.15	1.39	1.11	0.38	0.04
Satellite std dev (g kg^{-1})	1.21	1.12	0.74	0.22	0.02
Correlation	0.55	0.36	0.54	0.59	0.52
Rms (g kg^{-1})	1.20	1.49	0.98	0.35	0.03
Bias (raob − sat) (g kg^{-1})	−0.41	−0.41	−0.22	0.16	0.01

large mean fluxes in the lower atmosphere are caused by the unrealistically strong annual-mean winds (see Table 1).

Table 3 also shows that the eddy moisture fluxes from the mass-conserved and nonmass-conserved satellite-derived winds are similar. Both are about 50% smaller than the raob values at 850 and 700 hPa. The vertically integrated eddy flux from the satellite data is about 45% smaller than the raob value. Note that the annually averaged eddy flux, denoted by M_e, can be expressed as

$$M_e = \overline{v'q'} = r(v, q)\sqrt{\overline{v'^2}}\sqrt{\overline{q'^2}}, \qquad (14)$$

where q is the specific humidity, $\sqrt{\overline{v'^2}}$ and $\sqrt{\overline{q'^2}}$ are

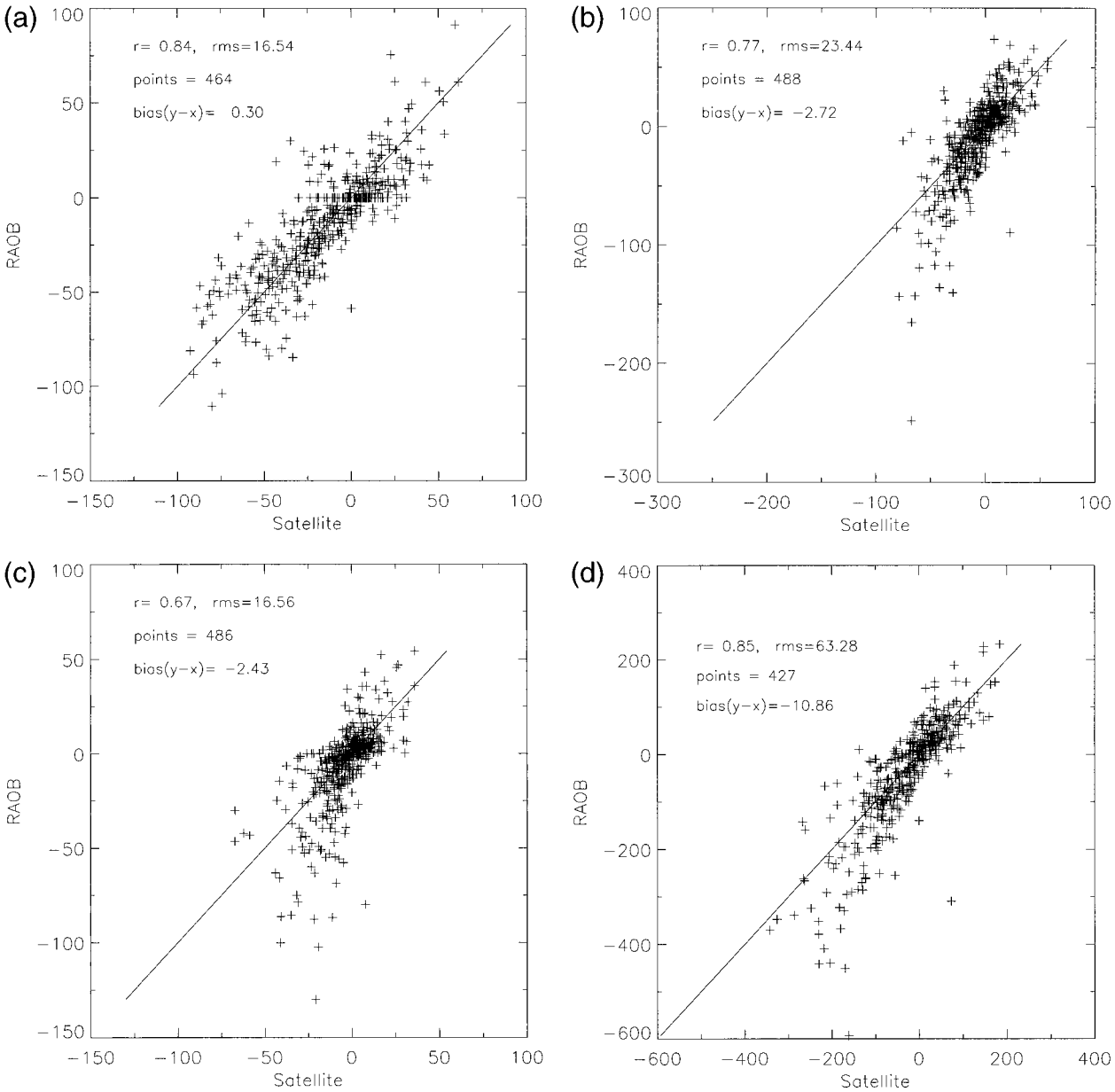

FIG. 5. Scatterplots of the satellite-derived, mass-conserved meridional moisture flux vs radiosonde observations for 1988: (a) 1000, (b) 850, and (c) 700 hPa, and (d) vertically integrated. Units for (a), (b), and (c): m s^{-1} g kg^{-1} and for (d): m^{-1} s^{-1}.

TABLE 3. Moisture flux statistics for the raob and satellite-derived data at Macquarie Island for 1988. The unit of the moisture flux at each level is: m s^{-1} g kg^{-1}; the vertically integrated moisture flux unit is kg m^{-1} s^{-1}.

	Height					
	1000 mb	850 mb	700 mb	500 mb	300 mb	Vert. integrated
Mean flux, raob	−10.77	−4.04	−1.88	−0.52	−0.10	−19.03
Mean flux, this study	−11.71	−3.35	−1.62	−0.33	−0.05	−17.78
Mean flux, SVW99	−11.71	−8.59	−4.61	−0.97	−0.11	−32.52
Eddy flux, raob	−3.37	−4.47	−4.06	−1.73	−0.21	−21.34
Eddy flux, this study	−2.73	−2.43	−1.92	−0.56	−0.04	−11.73
Eddy flux, SVW99	−2.73	−2.57	−1.99	−0.62	−0.04	−12.14
Total flux, raob	−14.14	−8.51	−5.98	−2.25	−0.31	−40.37
Total flux, this study	−14.44	−5.79	−3.55	−0.90	−0.09	−29.51
Total flux, SVW99	−14.44	−11.16	−6.61	−1.59	−0.15	−44.65
Correlation (raob, this study)	0.84	0.77	0.67	0.61	0.64	0.85
Correlation (raob, SVW99)	0.84	0.77	0.67	0.61	0.64	0.84

the standard deviations of the wind and specific humidity, respectively, and $r(v, q)$ is the correlation coefficient between the wind and moisture measurements. Table 4 lists the values of $r(v, q)$ for the raob measurements and satellite observations at different levels. From Tables 1, 2, and 4 it is seen that the satellite values of all three quantities of $\sqrt{\overline{v'^2}}$, $\sqrt{\overline{q'^2}}$, and $r(v, q)$ are smaller than the raob counterparts, which results in smaller eddy moisture fluxes from the satellite observations. As mentioned earlier, the smaller satellite $\sqrt{\overline{v'^2}}$ could be due either to temporal and spatial averaging or the lack of certain types of ageostrophic wind components. Temporal and spatial average may also result in a smaller $\sqrt{\overline{q'^2}}$. As a result, it is anticipated that future satellite observations with higher spatial and temporal resolution will improve the estimation of the eddy moisture flux.

The satellite-derived, vertically integrated total moisture flux with conservation of mass is −29.5 kg m^{-1} s^{-1}, a 27% underestimation as compared with the raob value of −40.4 kg m^{-1} s^{-1}. The underestimation is primarily caused by the underestimation of the eddy flux. The satellite-derived nonmass-conserved wind gives a vertically integrated total moisture flux that is closer to the raob value because the underestimated eddy flux is largely offset by the overestimated mean flux.

The above comparisons suggest that the satellite-derived mean moisture flux with conservation of mass is comparable to the raob values; however, the eddy flux is underestimated by about 45%.

5. Annual-mean climatology of the moisture fluxes for 1988

a. Zonally averaged moisture transport

Figures 6a–c show the vertical–latitudinal cross section of the satellite-derived, 1988 yearly and zonally averaged mean, eddy, and total moisture fluxes, respectively. Figure 7 provides the vertical profile of the annually and zonally averaged mean, eddy and total moisture fluxes, respectively, at 50°S. In the figures, the moisture fluxes are represented by the specific humidity fluxes, not the layer precipitable water fluxes, as used in SVW99. We have chosen to display the specific humidity flux field because it can be directly compared with other historical studies such as Oort and Peixóto (1983) and Bromwich et al. (1995). The specific humidity used in this flux calculation is obtained from the layer precipitable water based on the integral relationship between the two quantities. As in the moisture comparisons at Macquarie Island, the trapezoidal rule is used for the integration with the assumptions that the surface pressure is 1000 hPa and the specific humidity at 100 hPa is zero. This transformation may cause ~10% errors in the specific humidity flux field near the surface, poleward of 60°S, because the climatological surface pressure is typically around 980 hPa in this region. However, this transformation does not influence the layer-integrated moisture fluxes. For instance, by using the layer precipitable water and the nonmass-conserved satellite wind, SVW99 obtained a value of −15.1 kg m^{-1} s^{-1} for the vertically integrated, zonally averaged moisture flux across 60°S, which is exactly the same as that obtained in this study using the specific humidity profile and the nonmass-conserved satellite wind. From the figures, it is seen that for the mean flux, most transports occur in the planetary boundary layer due to the strong annual-mean boundary flows as shown in Fig. 1b. It reaches its maximum at the surface and decreases sharply with increasing height. Above the planetary boundary layer the mean moisture flux is negligible compared to the eddy moisture flux. As will be shown later, cancellation between the equatorward flux and poleward flux

TABLE 4. Correlation coefficient between v and q for the raob and satellite data at Macquarie Island for 1988.

	Height				
	1000 mb	850 mb	700 mb	500 mb	300 mb
Raob $r(v, q)$	−0.57	−0.36	−0.34	−0.34	−0.27
Satellite $r(v, q)$	−0.41	−0.38	−0.30	−0.19	−0.18

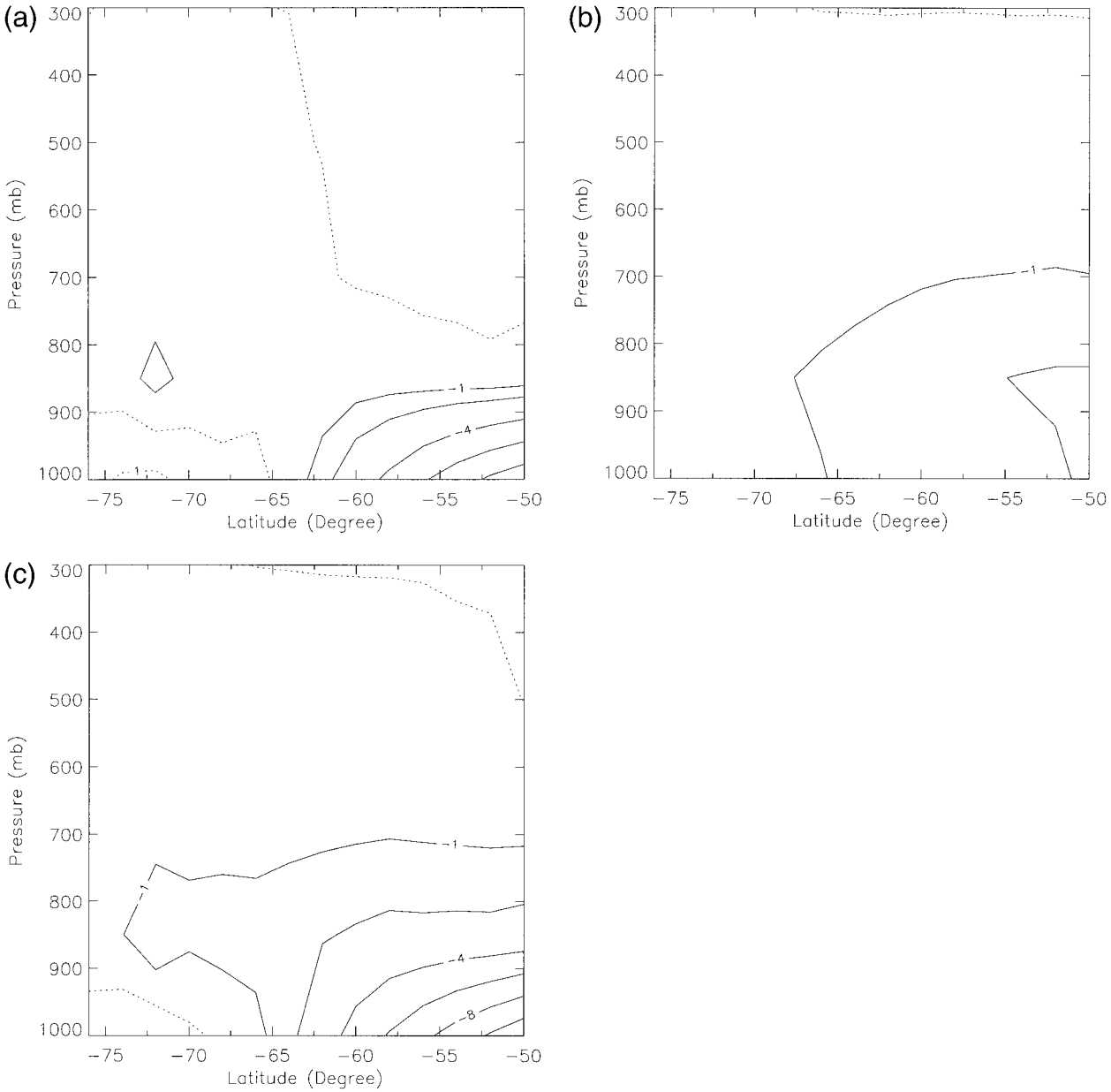

FIG. 6. Latitude–altitude cross sections for the 1988 annually and zonally averaged (a) mean, (b) eddy, and (c) total moisture transport (m s^{-1} g kg^{-1}).

at different longitudes causes the small zonally averaged mean moisture fluxes above the boundary layer.

Figures 8a–c show comparisons of the annually and zonally averaged, vertically integrated meridional moisture fluxes from this and other published studies. It shows that the mean moisture flux derived in this study is comparable to the ECMWF and NMC reanalyses (Bromwich et al. 1995) and the Peixóto and Oort (1983) results. In contrast, the mean flux of SVW99 is overestimated equatorward of 63°S and the latitudinal gradient is steeper than other reported values. For the latitude band from 50°S to 55°S, the eddy fluxes from both this study and the SVW99 study are underestimated by about 62% as compared with the ECMWF and NMC analyses and by 45% as compared with the Peixóto and Oort (1983) analysis. This underestimation is similar to the radiosonde comparison at Macquarie Island in section 4. Because of this underestimation, the total transport in this study is smaller than other reported values. In contrast, the total flux in SVW99 is larger than the other transport estimates because of compensation by the overestimated mean flux. In SVW99, the total flux

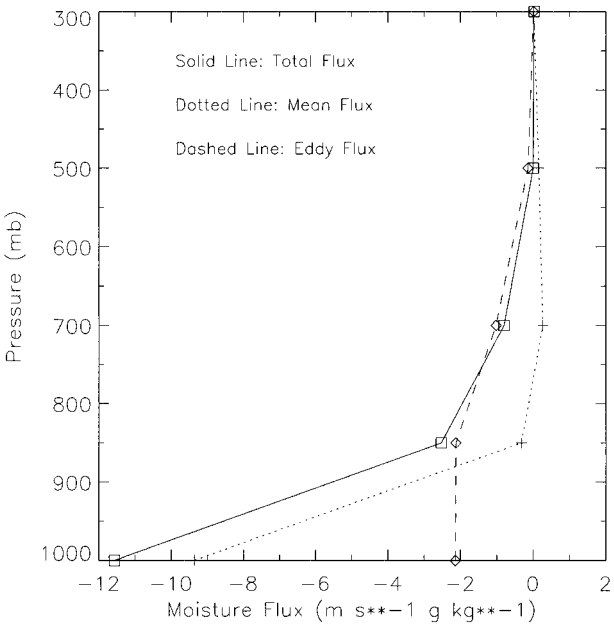

FIG. 7. Vertical profiles of the 1988 annually and zonally averaged moisture transport at 50°S. The solid line is the total transport, the dotted line is the mean transport, and the dashed line is the eddy transport.

across 50°S is -31.8 kg m^{-1} s^{-1}; the value from this study is -14.1 kg m^{-1} s^{-1}, a 56% reduction.

b. Latitudinal–longitudinal distribution

SVW99 described in detail the longitudinal dependence of the satellite-derived meridional moisture transport based on a nonmass-conserved wind field. In order to see the impact of the conservation of mass on the longitudinal variations of the moisture fluxes, Figs. 9a,b show the vertically integrated mean moisture transport of this study and the SVW99 counterpart, respectively. Figures 10 and 11 are similar to Fig. 9 but for eddy transport and total transport, respectively. It is seen that the longitudinal structure of the total flux in this study is similar to SVW99 except the transport is much weaker than SVW99. The structure and amplitude of the eddy transport are almost the same between the two studies. For the mean moisture transport, this study exhibits a maximum equatorward transport of about 30 kg m^{-1} s^{-1} over the Drake Passage and Scotia Sea. This is much stronger than the SVW99 value of 20 kg m^{-1} s^{-1}. In addition, the equatorward transport of the mean moisture flux in this study extends into the Southern Indian Ocean with values around 5–10 kg m^{-1} s^{-1}. In contrast, the mean equatorward moisture transports in SVW99

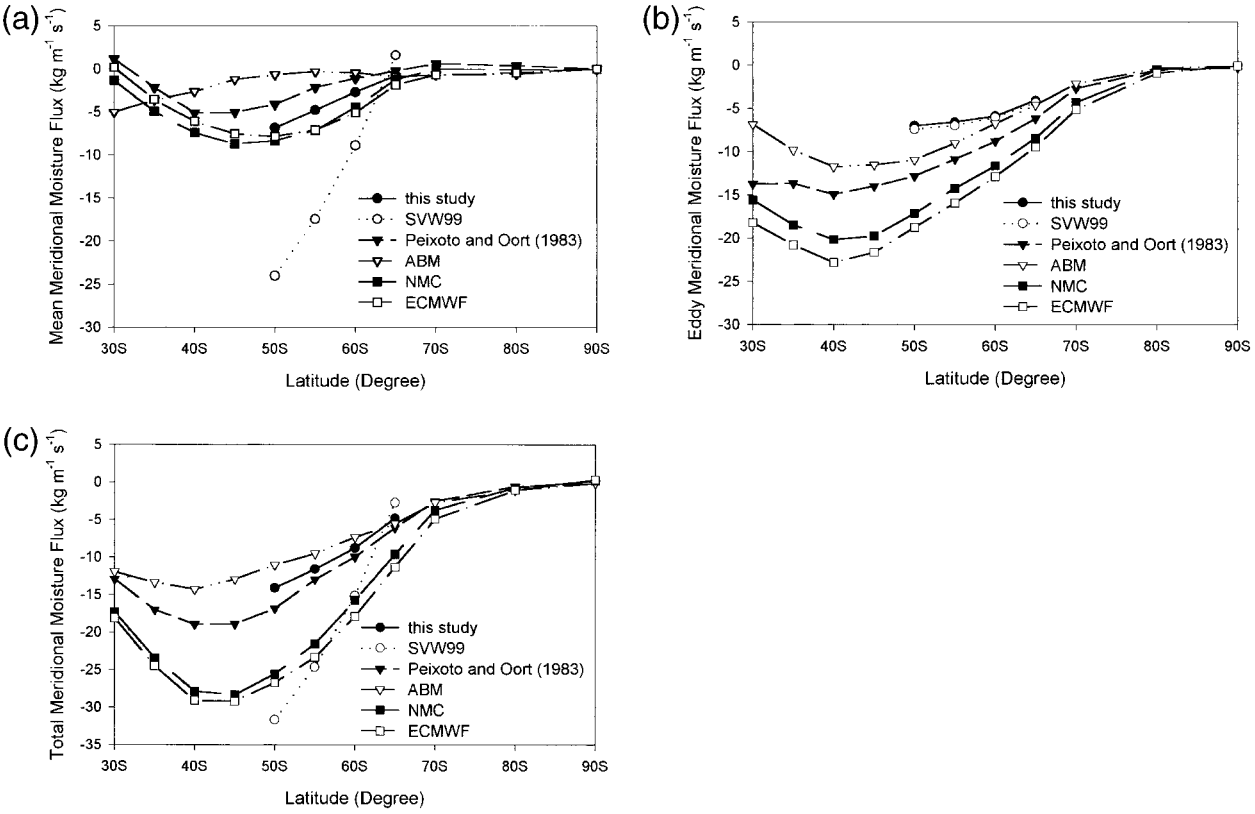

FIG. 8. Comparisons of the yearly and zonally averaged meridional moisture transport for different studies. ECMWF, NMC, and ABM analyses data are for the period of 1985–92 (Bromwich et al. 1995), Peixóto and Oort (1983) data are for the period of 1963–73, and SVW99 and this study are for 1988: (a) mean flux, (b) eddy flux, (c) total flux.

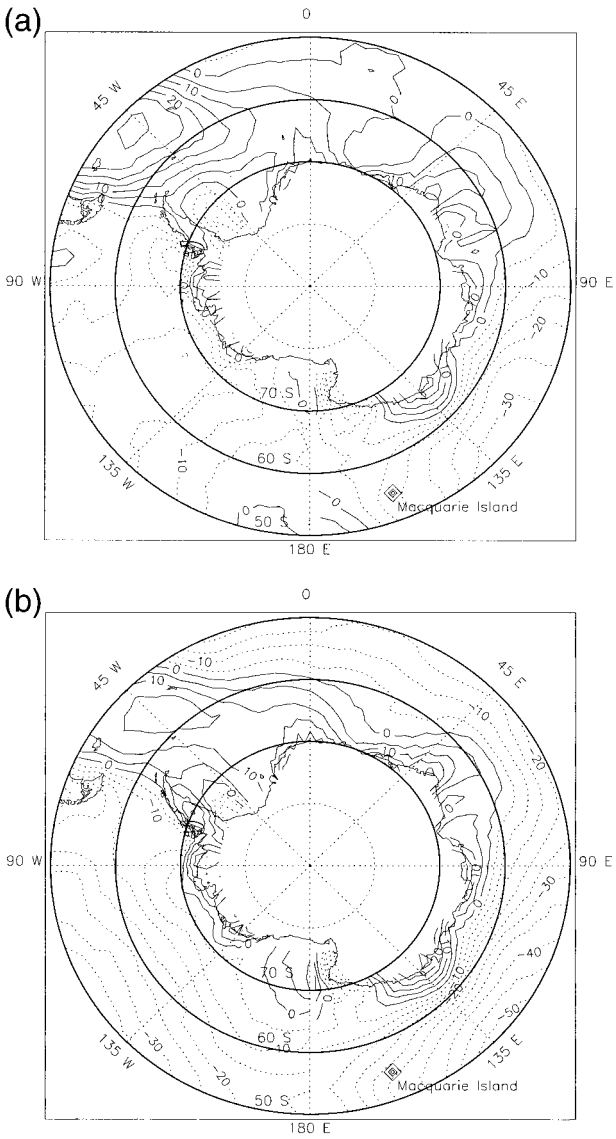

FIG. 9. Distribution of the annually averaged, vertically integrated mean meridional moisture fluxes (kg m^{-1} s^{-1}) for 1988 from the satellite data derived by (a) the mass-conserved approach and (b) the SVW99 approach. The figures are smoothed using a 5-point running-mean in the zonal direction.

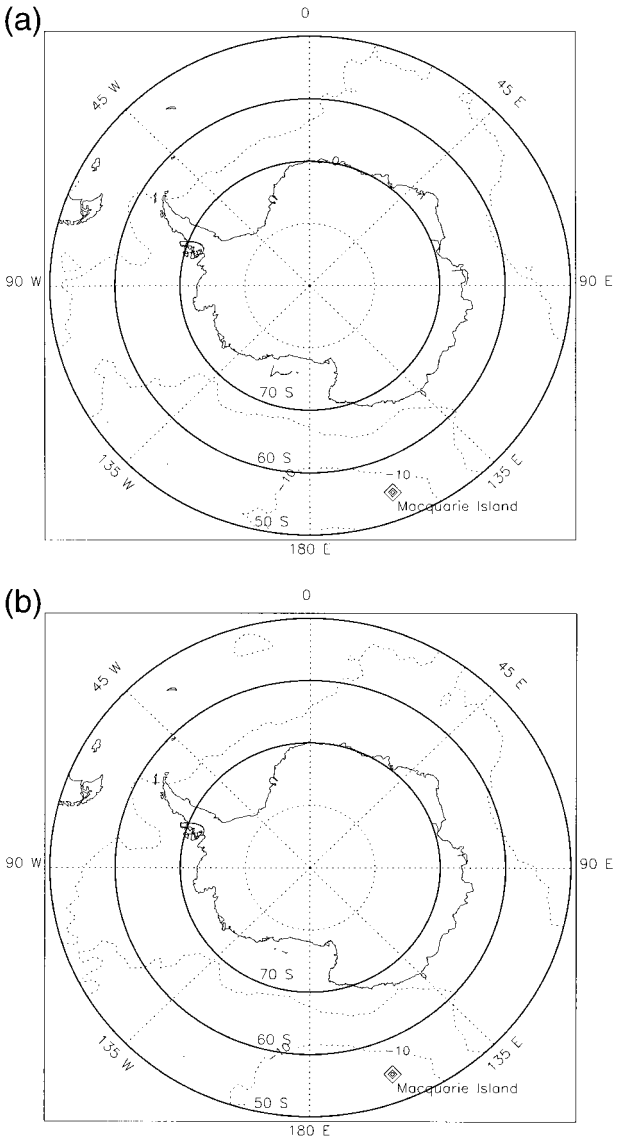

FIG. 10. Same as Fig. 9, but for the eddy moisture fluxes.

cover a much smaller area. The poleward transport by the mean wind in this study is much weaker than SVW99 over most ocean areas. For instance, over the Indian Ocean south of Australia, the poleward transport by the mean wind in SVW99 reaches 60 kg m^{-1} s^{-1}, while the value of this study is only around 30 kg m^{-1} s^{-1}.

As discussed before, the mean moisture transport is dominated by the planetary boundary layer flows. Figures 12a,b show the satellite-derived, annually averaged meridional winds at the surface and 850 hPa, respectively. The vertically integrated mean transport portrays many of the same characteristics as the 850-hPa wind. For instance, from the Drake Passage to the Southern Indian Ocean, the 850-hPa winds are equatorward, causing equatorward mean moisture transport. Near the continental coasts there are strong katabatic winds blowing off of the continent. Parish and Bromwich (1991) simulated the continental-scale katabatic winds over Antarctica and found strong katabatic winds along most of the coasts. Bromwich (1989) and Bromwich et al. (1992) studied the strong katabatic winds along the continental coast using satellite images. Both Figs. 12a,b show strong continental drainage flows. Off the northern edge of the Ross Ice Shelf, Filchner-Ronne Ice Shelf, and Amery Ice Shelf, the 850-hPa velocity field shows strong poleward flows while the 1000-hPa velocity field shows equatorward flows. The southerly surface winds over the Ross Ice Shelf and Ross Sea are described by many authors as the mountain-parallel flows that parallel

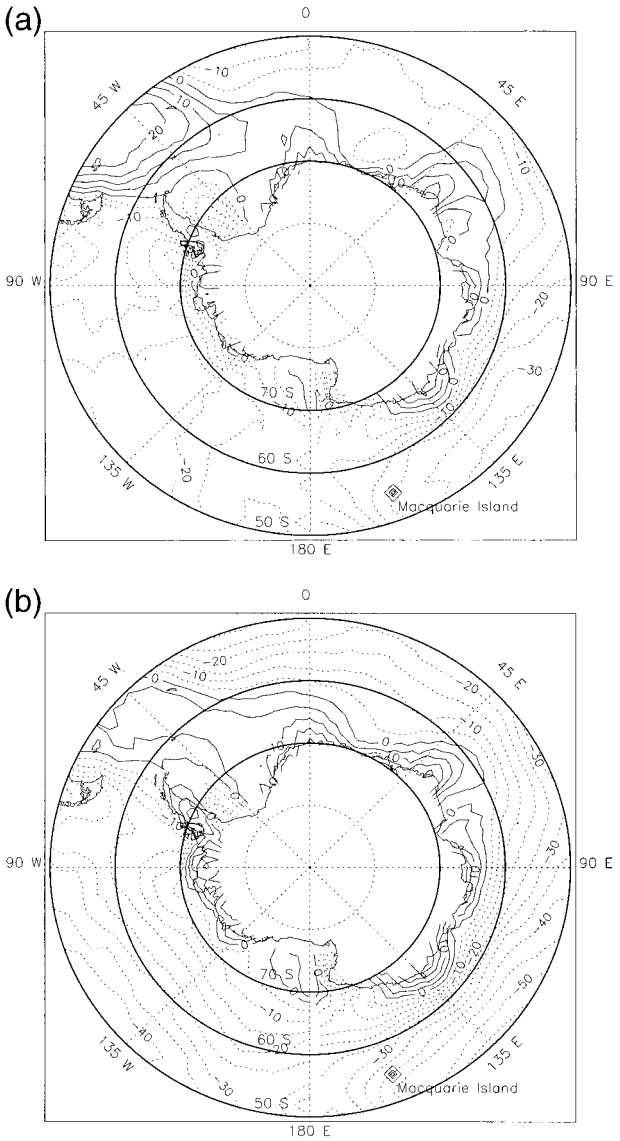

FIG. 11. Same as Fig. 9, but for the total moisture fluxes.

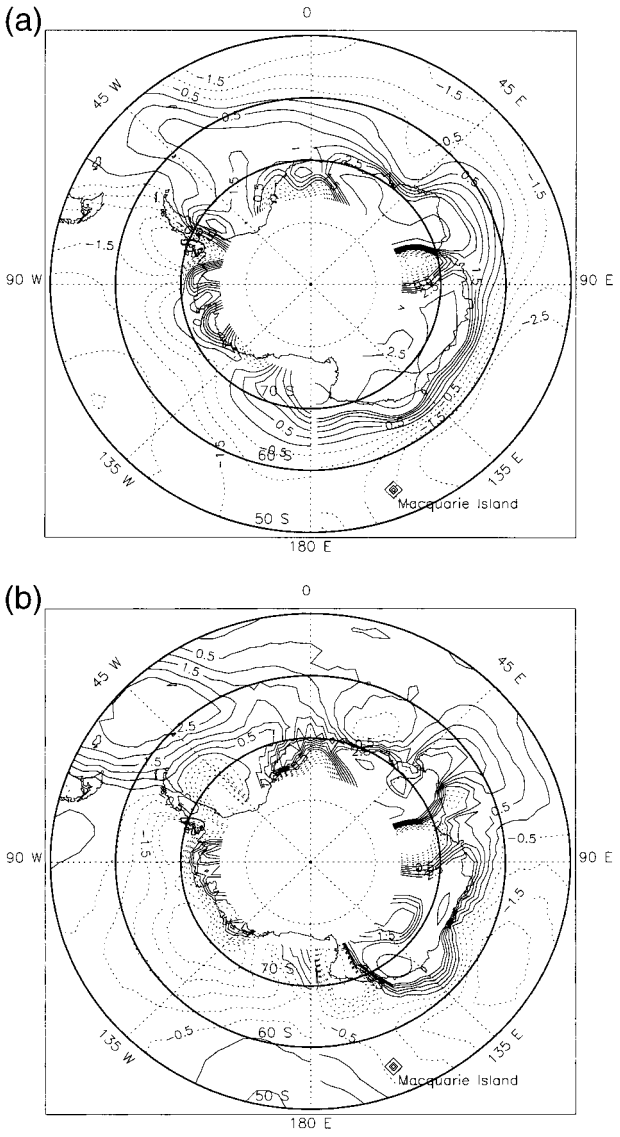

FIG. 12. 1988 annually average meridional winds based on the mass-conserved approach at (a) 1000 and (b) 850 hPa (m s^{-1}). The figures are smoothed using a 5-point running-mean in the zonal direction.

the Transantarctic Mountains (e.g., O'Connor and Bromwich 1988; Bromwich et al. 1993). The sharp reversal in the wind direction as height increases may be related to the cold air advection and temperature inversion near the surface (Parish and Bromwich 1991). These strong poleward winds at 850 hPa cause strong poleward moisture transport near the ice shelves.

Another interesting phenomenon is that the eddy transport is not totally in phase with the mean transport. The eddy transport is poleward almost everywhere over the Southern Ocean except near the ice shelves (e.g., over the Ross Sea near the Ross Ice Shelf). In particular, over the Drake Passage and Scotia Sea, the mean moisture flux is equatorward while the eddy moisture flux is poleward. This probably occurs because the mean flux and the eddy flux are controlled by different mechanisms. As discussed earlier, the mean flux is controlled by the flows in the planetary boundary layer, while the eddy flux is related to the vertically integrated meridional temperature gradient (Stone and Yao 1990).

Because of the complicated phase relationship between the eddy and mean fluxes, the total moisture transport exhibits features different from either the eddy or the mean fluxes. Over the Scotia Sea, the total equatorward moisture transport is weakened because of the cancellation between the eddy and mean fluxes, while over the Southern Indian Ocean, the total poleward transport is strengthened due to the poleward transport by both mean and eddy winds. Over most of the Southern Ocean, the poleward total moisture transport is

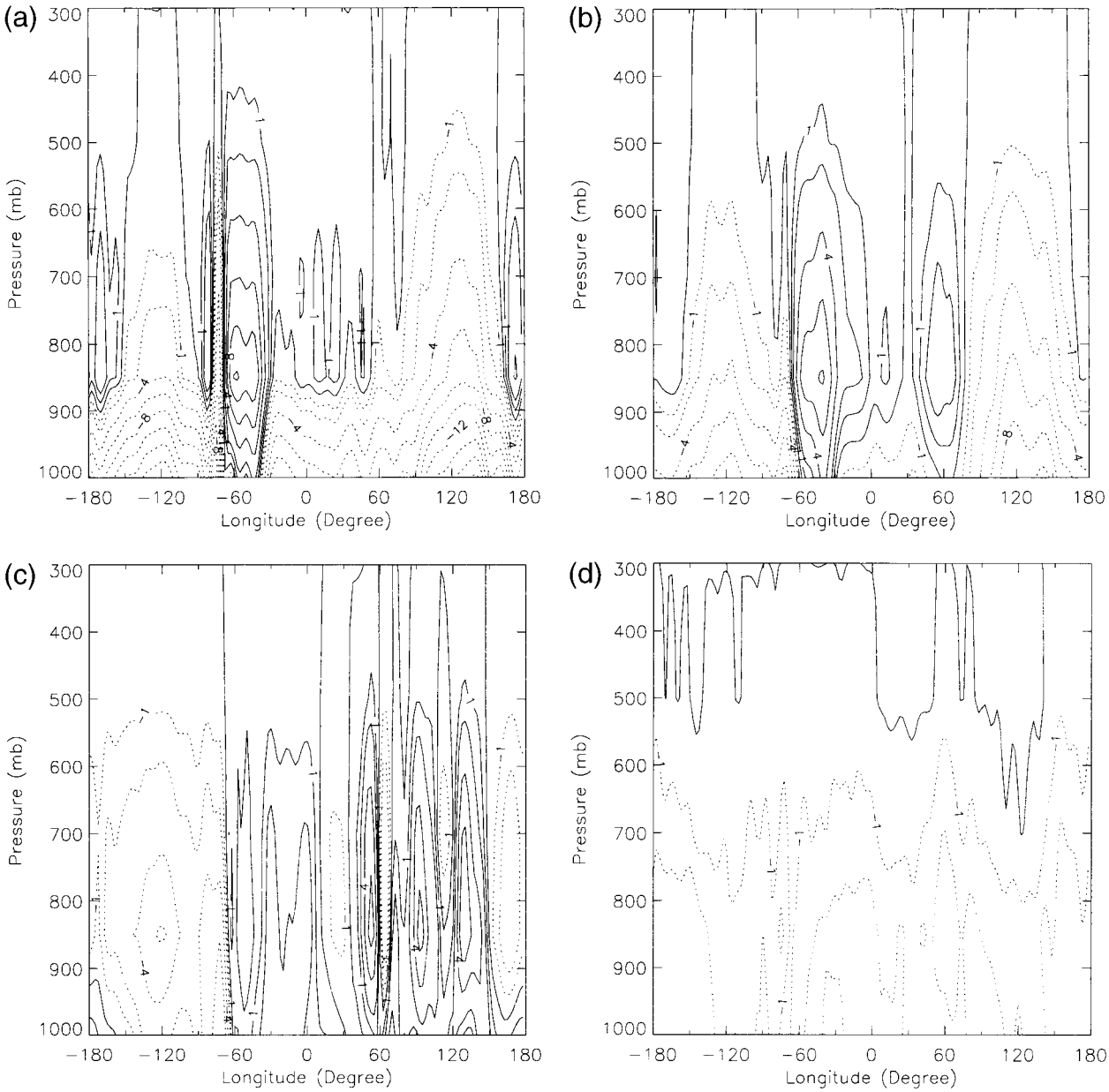

FIG. 13. 1988 longitude–altitude cross sections of the satellite-derived, annually averaged meridional moisture fluxes using the mass-conserved wind: (a) mean flux at 50°S; (b) mean flux at 58°S; (c) mean flux at 66°S; (d) eddy flux at 50°S; (e) eddy flux at 58°S; (f) eddy flux at 66°S. The figures are smoothed using a 5-point running-mean in the zonal direction. Units: m s^{-1} g kg^{-1}.

strengthened when the eddy flux and mean flux are in phase. However, because the eddy flux is underestimated in this study, it is possible that an increase in the amplitude of the eddy fluxes could lead to a weakening of the total equatorward transport or even a shift to poleward flow. Better estimates of the eddy moisture flux are required to resolve this uncertainty.

c. Vertical and longitudinal distribution

Vertical–longitudinal cross sections of the moisture transport reveal additional three-dimensional features of the moisture transport across the Southern Ocean. Figures 13a–f show the vertical–longitudinal cross section of the moisture transports by the mean and eddy winds at 50°S, 58°S, and 66°S, respectively. At 50°S (Fig. 13a), the mean equatorward transport occurs over the Scotia Sea and Drake Passage (30°–70°W) with a maximum near the top of the boundary layer. As latitude increases to 58°S (Fig. 13b), the mean transport over the South Atlantic Ocean and part of the Indian Ocean (30°W to 75°E) also becomes equatorward. At 66°S (Fig. 13c) the mean transport becomes equatorward over the whole latitudinal belt except for the South Pacific sector; both

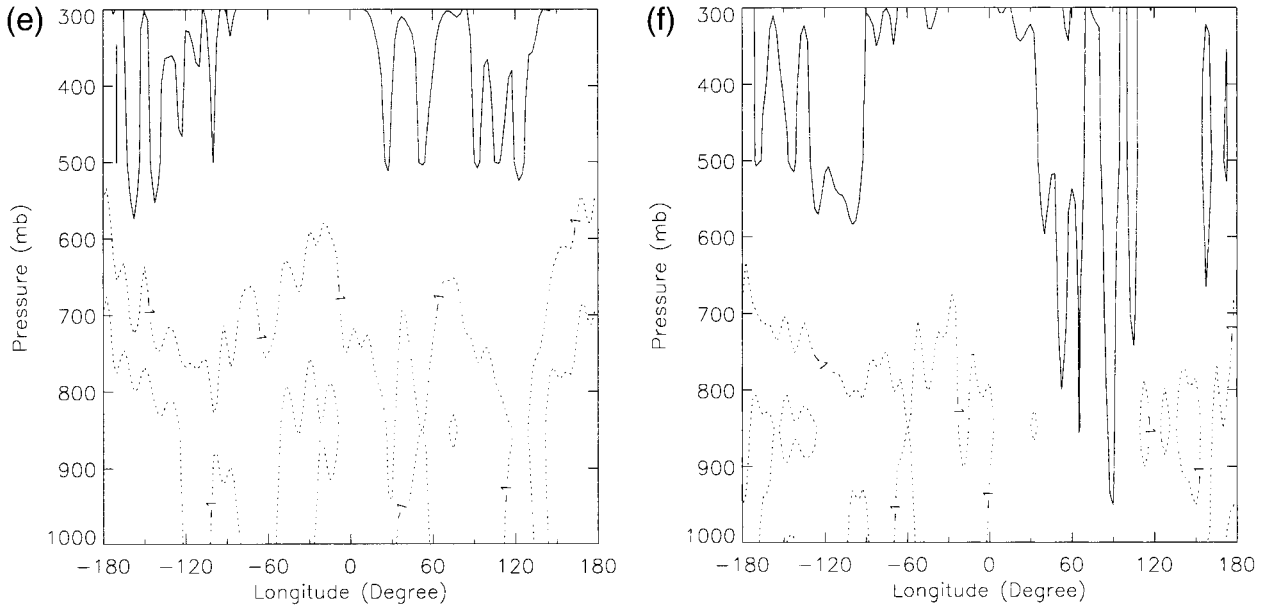

FIG. 13. (*Continued*)

eddy and mean moisture transports are poleward over the South Pacific sector. However, at higher latitudes (e.g., 76°S, not shown here), both eddy and mean moisture transports over the South Pacific sector also becomes equatorward. In Fig. 7, a rather small zonally averaged mean moisture flux is observed above 850 hPa. From Fig. 13a it is seen that the small zonally averaged mean flux above 850 hPa is due to the cancellation of the equatorward transport over the Scotia Sea, South Atlantic Ocean, and southwest Pacific Ocean and the poleward transport over the rest of the latitude belt. This feature also occurs at other latitudes and is consistent with the work of Bromwich (1988) and Peixóto and Oort (1983) who found that averaging in longitude results in a smaller mean flux because of cancellation.

Though the satellite-derived eddy moisture fluxes tend to underestimate the true values, some general features can still be learned from the figures. As noted before, the eddy transport is not totally in phase with the mean transport. Poleward moisture transport is observed at all longitudes below 600 hPa from 50°S to 58°S (Figs. 13d,e). This gives a dominant zonally averaged eddy flux above the boundary layer as shown in Fig. 7. The longitudinal distribution of the eddy flux is quite uniform. Stone and Yao (1990) indicate that the zonally averaged eddy moisture flux is related to the vertically averaged meridional temperature gradient with a synoptic wave-scale exponential decay as the weighting function. The longitudinal uniformity of the eddy moisture flux suggests that the zonally averaged dynamics might be a good approximation for describing the three-dimensional structure of the eddy moisture fluxes.

6. Net precipitation

Seasonal to interannual timescale net precipitation can be estimated using the water vapor budget equation. This method has been used by many authors (e.g., Bromwich et al. 1995; Cullather et al. 1998; SVW99). The budget equation for the temporally and spatially averaged atmospheric moisture is

$$\langle \overline{P} - \overline{E} \rangle = -\langle \nabla \cdot \overline{\mathbf{M}} \rangle - \langle d\overline{W}/dt \rangle, \tag{15}$$

where the angle brackets represent spatial average, the bar a time average, P precipitation/snow, E evaporation/sublimation, W the precipitable water, and $\mathbf{M}$ the vertically integrated total moisture flux. For long-term averages, the moisture storage term can be neglected so the net precipitation $\langle \overline{P} - \overline{E} \rangle$ is solely determined by the convergence of the moisture fluxes. Because only the meridional wind is derived from the satellite observations in this study, only zonally averaged net precipitation can be estimated. The zonally averaged net precipitation equation is

$$\langle \overline{P} - \overline{E} \rangle = -\int_0^{p_0} \frac{1}{a \cos\varphi} \frac{\partial}{\partial \varphi} [\cos\varphi (\langle \overline{v} \rangle \langle \overline{q} \rangle + \langle \overline{v'q'} \rangle)] \frac{dp}{g}, \tag{16}$$

where the brackets represent the zonal average, the primes represent departures from the zonal average, and g is the gravity constant.

Table 5 provides a comparison of the net precipitation in the latitude belt from 50° to 60°S based on the work of various authors. Note that the cited authors did not provide the separation between the eddy and mean flux convergence. The separation is calculated in this study

TABLE 5. Zonally averaged net precipitation estimates (mm yr^{-1}) by different authors.

Study	50°–60°S		
	Mean	Eddy	Total
This study	154	78	232
SVW99	547	87	634
NMC (Bromwich et al. 1995)	156	258	414
ECMWF (Bromwich et al. 1995)	123	279	402
ABM (Bromwich et al. 1995)	11	181	192
Peixóto and Oort (1983)	104	190	294
Howarth (1983)			160
Starr et al. (1969)			528

based on the retrieved flux data from the original authors, so 5%–10% errors may exist between the provided values and the original values. However, the errors do not affect the discussion below.

Comparing the net precipitation value of 634 mm yr^{-1} by SVW99 with the value of 232 mm yr^{-1} in this study, it is seen that conservation of mass yields a 63% reduction in the estimation of the net precipitation. This difference is mainly caused by the difference in the mean flux. As seen in Fig. 8a, the larger meridional gradient and larger values of the mean moisture flux around 50°S and 60°S by SVW99 causes larger convergence of the mean moisture flux.

Table 5 shows that there is a favorable agreement in the convergence of the mean moisture fluxes among NMC, ECMWF, and the current study, with a difference less than 20%. Other studies show larger discrepancies in the convergence of the mean moisture fluxes. This is probably because of difficulties in obtaining mean meridional winds at high latitudes, which involves cancellation of large amplitude instantaneous southerly and northerly winds. As a result, large errors can occur in the resultant small-amplitude annual-mean meridional wind. This is especially true of observations with limited spatial and temporal coverage. For instance, Oort and Peixóto (1983) did not use the observed estimates of zonal and annual-mean meridional wind for their flux calculations because of large errors in the zonally averaged meridional wind. Instead, they used a mean meridional wind obtained by solving the momentum balance equation. In this aspect, the analyses and the satellite data are more reliable because of higher spatial and temporal resolutions.

The contribution to the net precipitation from eddy moisture fluxes in both SVW99 and this study is lower than all other reported values. This is a result of the underestimated eddy fluxes discussed in previous sections.

7. Discussion and conclusions

A Lagrange multiplier is introduced to constrain the total mass in the satellite-derived meridional wind field obtained by using the thermal wind equation in conjunction with the satellite observed temperature profiles and VAM surface winds. The conservation of mass has made substantial improvements to the wind field, the mean moisture transport, and its convergence compared to the nonmass-conserved study of SVW99. The derived wind field reproduces the basic features of the annual-mean circulation of the atmosphere over the southern high latitudes. The satellite-derived mean moisture flux agrees with the radiosonde observations at Macquarie Island to within 6%. However, the eddy fluxes from both the mass-conserved and nonmass-conserved methods are 45% smaller than the radiosonde observations. The smaller eddy moisture flux is a result of the smaller temporal variability (standard deviations) of the moisture and meridional wind field, as well as a smaller correlation between the moisture and wind fields derived from the satellite data. The smaller variability of the satellite moisture and wind fields is most likely due to averaging of the satellite data in both space and time. The lack of certain ageostrophic components in the wind derivation may also cause lower instantaneous wind speeds. Therefore, improvements in the moisture and wind observations as well as the incorporation of higher order dynamics are necessary for future studies.

In the variational formalism, the zonally averaged mass conservation equation is used as a strong constraint. This choice of constraint results in a constant Lagrange multiplier on a latitude wall (the Lagrange multiplier is a function of latitude and time only). Other forms of mass conservation constraint may also be applied in the variational formalism. For instance, the vertically integrated mass conservation equation, which is often used in the data initialization for removing external gravity waves (e.g., Haltiner and Williams 1980), can also be used as a constraint. In this situation, however, the zonal wind and meridional wind components need to be solved simultaneously. The Lagrange multiplier will be a function of both latitude and longitude and controlled by Poisson's equation. Boundary conditions must be imposed to solve Poisson's equation. Typically, the natural boundary condition in which the Lagrange multiplier is set to zero at the boundaries is used (e.g., Shapiro and Mewes 1999). Because the Lagrange multiplier is a function of both latitude and longitude, more refinements on the latitude circle can probably be achieved compared to the constraint of the zonally averaged mass conservation. However, the wind correction using this constraint requires the calculation of the wind divergence, which will most likely amplify errors in the dataset. In contrast, the zonally averaged mass conservation constraint developed here does not amplify the noise nor are boundary conditions for the Lagrange multiplier required. In addition, the zonally averaged mass conservation yields fairly reasonable annual-mean wind profiles at Macquarie Island, even though the Lagrange multiplier is longitudinally independent. We have chosen this constraint because it is

the simplest constraint that yields results consistent with raob data at Macquarie Island and reanalysis products.

The results of this study are subject to many of the same limitations as the TOVS data (Susskind 1993). In particular, temperature and moisture soundings are obtained only under clear or partially cloudy (up to 80%) conditions (Susskind 1993); no retrievals were made for totally overcast conditions. In SWV99 and this study, missing data in the subsequent thermal wind are replaced by interpolated values based on nearby good data. In many situations, the good data can be far away from the locations of the missing data. It is unclear how these interpolated data affect the results presented in this study; therefore, further sensitivity studies are required to fully resolve such questions.

Acknowledgments. Joel Susskind and Paul Piraino provided the TOVS Path A data. Robert Atlas and Joe Ardizzone provided the SSM/I-derived surface wind vector fields. Yuejian Zhu provided the NCEP–NCAR reanalysis data. The ECMWF data were obtained from UCAR. Their efforts in producing these datasets are greatly appreciated. We also thank Richard Slonaker for many thoughtful comments and discussions during the development of this project. We are grateful to the comments and suggestions of the two anonymous reviewers. This study was supported by NASA Grant W18 795 to the second author.

REFERENCES

Arnold, J. E., J. R. Scoggins, and H. E. Fuelberg, 1976: A comparison between *Nimbus-5* THIR and ITPR temperatures and derived winds with rawinsonde data obtained in the AVE II experiment. NASA Contractor Rep. CR-2757, 76 pp.

Atlas, R., R. N. Hoffman, and S. C. Bloom, 1993: Surface wind velocity over the oceans. *Atlas of Satellite Observations Related to Global Change,* R. J. Gurney, J. L. Foster, and C. L. Parkinson, Eds., Cambridge University Press, 129–139.

——, R. N. Hoffman, S. C. Bloom, J. C. Jusem, and J. Ardizzone, 1996: A multi-year global surface wind velocity dataset using SSM/I wind observations. *Bull. Amer. Meteor. Soc.,* **77,** 869–882.

Bluestein, H. B., 1993: *Observations and Theory of Weather Systems.* Vol. II. *Synoptic-Dynamic Meteorology in Midlatitudes,* Oxford University Press, 594 pp.

Boville, B. A., 1987: The validity of the geostrophic approximation in the winter stratosphere and troposphere. *J. Atmos. Sci.,* **44,** 443–457.

Bromwich, D. H., 1988: Snowfall in high southern latitudes. *Rev. Geophys.,* **26,** 149–168.

——, 1989: Satellite analyses of Antarctic katabatic wind behavior. *Bull. Amer. Meteor. Soc.,* **70,** 738–749.

——, J. F. Carrasco, and C. R. Stearns, 1992: Satellite observations of katabatic-wind propagation for great distances across the Ross Ice Shelf. *Mon. Wea. Rev.,* **120,** 1940–1949.

——, T. R. Parish, A. Pellegrini, C. R. Stearns, and G. A. Weidner, 1993: Spatial and temporal characteristics of the intense katabatic winds at Terra Nova Bay. *Antarctica, Antarctic Meteorology and Climatology: Studies Based on Automatic Weather Stations,* D. H. Bromwich and C. R. Sterns, Eds., American Geophysical Union, 47–68.

——, F. M. Robasky, R. I. Cullather, and M. L. Van Woert, 1995: The atmospheric hydrologic cycle over the Southern Ocean and Antarctica from operational numerical analyses. *Mon. Wea. Rev.,* **123,** 3518–3538.

——, A. N. Rogers, P. Kållberg, R. I. Cullather, J. W. C. White, and K. J. Kreutz, 2000: ECMWF analyses and reanalyses depiction of ENSO signal in Antarctic precipitation. *J. Climate,* **13,** 1406–1420.

Carle, W. E., and J. R. Scoggins, 1981: Determination of wind from *Nimbus 6* satellite sounding data. NASA Reference Publication 1072, 82 pp.

Cullather, R. I., D. H. Bromwich, and M. L. Van Woert, 1996: Interannual variations in Antarctic precipitation related to El Niño–Southern Oscillation. *J. Geophys. Res.,* **101,** 19 109–19 118.

——, ——, and ——, 1998: Spatial and temporal variability of Antarctic precipitation from atmospheric methods. *J. Climate,* **11,** 334–367.

Daley, R., 1991: *Atmospheric Data Analysis.* Cambridge University Press, 457 pp.

Douglas, B. C., 1991: Global sea level rise. *J. Geophys. Res.,* **96,** 6981–6992.

Francis, J. A., 1994: Improvements to TOVS retrievals over sea ice and applications to estimating Arctic energy fluxes. *J. Geophys. Res.,* **99,** 10 395–10 408.

Gent, P. R., and J. C. McWilliams, 1983: Consistent balanced models in bounded and periodic domains. *Dyn. Atmos. Oceans,* **7,** 67–93.

Genthon, C., and G. Krinner, 1998: Convergence and disposal of energy and moisture on the Antarctic polar cap from ECMWF reanalyses and forecasts. *J. Climate,* **11,** 1073–1716.

Gibson, R., P. Kallberg, and S. Uppala, 1996: The ECMWF re-analysis (ERA) project. *ECMWF Newsl.,* **73,** 7–17.

Gruber, A., and J. J. O'Brien, 1968: An objective analysis of wind data for energy budget Studies. *J. Appl. Meteor.,* **7,** 333–338.

Haltiner, G. J., and R. T. Williams, 1980: *Numerical Prediction and Dynamic Meteorology.* John Wiley and Sons, 477 pp.

Howarth, D. A., 1983: Seasonal variations in the vertically integrated water vapor transport fields over the Southern Hemisphere. *Mon. Wea. Rev.,* **111,** 1259–1272.

Huang, J., and K. Bowman, 1992: The small ice cap instability in seasonal energy balance models. *Climate Dyn.,* **7,** 205–215.

Jacobs, S. S., H. H. Helmer, C. S. M. Doake, A. Jenkins, and R. M. Frolich, 1992: Melting of ice shelves and the mass balance of Antarctica. *J. Glaciol.,* **38,** 975–987.

Kalnay, E., and Coauthors, 1996: The NCEP/NCAR 40-Year Reanalysis Project. *Bull. Amer. Meteor. Soc.,* **77,** 437–471.

Moyer, V., J. R. Scoggins, N.-M. Chou, and G. S. Wilson, 1978: Atmospheric structure deduced from routine *Nimbus 6* satellite data. *Mon. Wea. Rev.,* **106,** 1340–1352.

O'Conner, W. P., and D. H. Bromwich, 1988: Surface airflow around Windless Bight, Ross Island, Antarctica. *Quart. J. Roy. Meteor. Soc.,* **114,** 917–938.

Oort, A. H., and J. P. Peixóto, 1983: Global angular momentum and energy balance requirements from observations. *Advances in Geophysics,* Vol. 25, Academic Press, 355–490.

Parish, T. R., and D. H. Bromwich, 1991: Continental-scale simulation of the Antarctic katabatic wind regime. *J. Climate,* **4,** 135–146.

Peixóto, J. P., and A. H. Oort, 1983: The atmospheric branch of the hydrological cycle and climate. *Variations in the Global Water Budget,* A. Street-Perrott, M. Beran, and R. Ratcliffe, Eds., D. Reidel, 5–65.

——, and ——, 1992: *Physics of Climate.* American Institute of Physics, 520 pp.

Peterson, R. A., and L. H. Horn, 1977: An evaluation of 500 mb height and geostrophic wind fields derived from *Nimbus-6* soundings. *Bull. Amer. Meteor. Soc.,* **58,** 1195–1201.

Reuter, D., J. Susskind, and A. Pursch, 1988: First-guess dependence of a physically based set of temperature-humidity retrievals from HIRS2/MSU data. *J. Atmos. Oceanic Technol.,* **5,** 70–83.

Shapiro, A., and J. Mewes, 1999: New formulations of dual-Doppler wind analysis. *J. Atmos. Oceanic Technol.,* **16,** 782–792.

Shapiro, M. A., and P. J. Kennedy, 1981: Research aircraft measure-

ments of jet stream geostrophic and ageostrophic winds. *J. Atmos. Sci.*, **38,** 2642–2652.

Slonaker, R. L., and M. L. Van Woert, 1999: Atmospheric moisture transport across the Southern Ocean via satellite observations. *J. Geophys. Res.*, **104,** 9229–9249.

Starr, V. P., J. P. Peixóto, and R. McKean, 1969: Pole-to-pole moisture conditions for the IGY. *Pure Appl. Geophys.*, **15,** 300–331.

Stone, P. H., and M.-S. Yao, 1990: Development of a two-dimensional zonally averaged statistical-dynamical model. Part III: The parameterization of the eddy fluxes of heat and moisture. *J. Climate*, **3,** 726–740.

Susskind, J., 1993: Water vapor and temperature. *Atlas of Satellite Observations Related to Global Change*, R. J. Gurney, J. L. Foster, and C. L. Parkinson, Eds., Cambridge University Press, 89–128.

——, P. Piraino, L. Rokke, L. Iredell, and A. Mehta, 1997: Characteristics of the TOVS Path A dataset. *Bull. Amer. Meteor. Soc.*, **78,** 1449–1472.

Wang, J. R., S. H. Melfi, P. Racette, D. N. Whitemen, L. A. Chang, R. A. Ferrare, K. D. Evans, and F. J. Schmidlin, 1995: Simultaneous measurements of atmospheric water vapor with MIR, Raman lidar, and rawinsonde. *J. Appl. Meteor.*, **34,** 1595–1607.